High-Temperature Rupture of 5083-Al Alloy under Multiaxial Stress States

Ho-Kyung Kim*, Duk-Kyu Chun
Department of Automotive Engineering, Seoul National University of Technology, 172 Kongnung-dong, Nowon-ku, Seoul 139-743, Korea
Sung-Hoon Kim
Department of Structural Engineering, Seoul National University of Technology, 172 Kongnung-dong, Nowon-ku, Seoul 139-743, Korea

High-temperature rupture behavior of 5083-Al alloy was tested for failure at 548K under multiaxial stress conditions : uniaxial tension using smooth bar specimens, biaxial shearing using double shear bar specimens, and triaxial tension using notched bar specimens. Rupture times were compared for uniaxial, biaxial, and triaxial stress conditions with respect to the maximum principal stress, the von Mises effective stress, and the principal facet stress. The results indicate that the von Mises effective and principal facet stresses give good correlation for the material investigated, and these parameters can predict creep life data under the multiaxial stress states with the rupture data obtained from specimens under the uniaxial stress. The results suggest that the creep rupture of this alloy under the testing condition is controlled by cavitation coupled with highly localized deformation process, such as grain boundary sliding. It is also conceivable that strain softening controls the highly localized deformation modes which result in cavitation damage in controlling rupture time of this alloy.

Key Words : Multiaxial Stress States, High-Temperature Rupture, Principal Facet Stress, Creep Cavitation, Damage Tolerance

1. Introduction

Intergranular creep fracture of structural components at elevated temperatures has been studied extensively for more than 30 years (Ridel, 1987). The fracture frequently occurs by the nucleation, growth and coalescence of intergranular cavities. This mode of failure has been studied, primarily under uniaxial stresses. However, the uniaxial stress experiments do not provide sufficient information to predict a creep rupture lifetime under the multiaxial stress state. Most components in service are subjected to a multiaxial stress system, because the multiaxial stress states are produced at notches and other geometric irregularities, even under remoted purely uniaxial loading. An incorrectly assumed multiaxial stress rupture criterion can result in a non-conservative design.

Several methods have been proposed for correlating creep life data for different multiaxial stress states (Hayhurst, 1972 ; Hayhurst et al., 1977 ; Kim et al., 1998 ; Henderson, 1979). Most of these methods are based on continuum mechanics arguments, while others are based on particular physical mechanisms which can influence grain boundary cavitation. Hayhurst (1972) has shown that for a smooth cylindrical specimen subjected to uniaxial tension, the rupture lifetime at a given temperature can be expressed as follows ;

* Corresponding Author,
E-mail : kimhk@snut.ac.kr
TEL : +82-2-970-6348; **FAX** : +82-2-979-7032
Department of Automotive Engineering, Seoul National University of Technology, 172 Kongnung-dong, Nowon-ku, Seoul 139-743, Korea. (Manuscript **Received** January 5, 2005; **Revised** June 2, 2005)

$$t_f = M\sigma^{-\chi} \quad (1)$$

where σ is the uniaxial stress and M and χ are parameters that characterize the evolution of damage at the temperature in equation. The need to consider the multiaxial stresses is demonstrated by the fact that Eq. (1) does not correctly predict creep rupture of notched bars even if the nominal stress in the notch is used in the expression (Hayhurst, 1972). Several parameters which contain adjustable constants have been proposed to correlate rupture times for the multiaxial stress states (Huddleston, 1985; Cane, 1982). However, the present work only considers the multiaxial stress parameters that are rigid in the sense that their determination does not involve adjustable terms. These stress parameters are briefly discussed below.

The Maximum Principal Stress. It is well known that the diffusive growth of intergranular cavities is driven by the tensile stresses acting normal to the grain boundaries. Thus, the role of the maximum principal stress, σMPS, will dominate high temperature rupture if cavity nucleation is easy and the cavities are homogeneously distributed on all grain boundaries. In this case, cavitation would not be constrained by creep deformation, and cavity growth rates would be limited only by the magnitude of the tensile stresses driving the diffusive cavity growth process.

The von Mises Effective Stress. For inhomogeneously distributed cavitation, the overall rate of the diffusive cavity growth process is governed by the creep rate of the surroundings (Dyson, 1976). In this case, the shear stresses that drive creep deformation should also have a role in governing the rate of cavity growth (Anderson and Rice, 1985). This provides the rationale for considering the von Mises effective stress, σ_{MPS}, as a correlating stress parameter for different stress states. It is also found that the success of σ_e in correlating rupture times for different stress states is also possible when the microstructural strain softening occurs during creep (Eggler, 1989).

The principal Facet Stress. This stress parameter proposed by Nix et al.(1989) was derived for correlating intergranular cavitation and creep rupture under the multiaxial stresses state. This approach is based on the average tensile stress on the grain boundary facets perpendicular to the maximum principal stress resulting from stress redistribution associated with the grain boundary sliding. Since stress distribution after the grain boundary sliding can significantly enhance the creep damage on the transverse facets that facilitates high temperature fracture, it is reasonable that the rupture life of the specimen is related to this parameter. This stress parameter, called the principal facet stress, is obtained by

$$\sigma_{PFS} = 2.24\sigma_1 - 0.62(\sigma_2 + \sigma_3) \quad (2)$$

where $\sigma_1 > \sigma_2 > \sigma_3$ are the principal stresses. This restricts the validity of the principal facet stress to rupture behavior which is influenced by grain boundary sliding mechanisms. This parameter has been shown to be consistent with creep rupture data for several alloys (Kim et al., 1998; Nix et al., 1989).

The 5083-Al alloy is a representative non-age-hardenable Al-Mg based alloy which possesses many interesting characteristics as a structural material, such as low price, fairly high strength, good corrosion resistance, high formability, etc. (Vetrano et al., 1994). These advantages of the alloy are quite attractive in the automotive industry for producing vehicles with high fuel efficiency by replacing steels with the alloy. In spite of the engineering significance of the 5083-Al alloy, there is still a lack of systematic studies on the high temperature rupture of 5083-Al alloy

Table 1 Stress analysis and stress parameters for the specimen geometry

		Uniaxial Tension	Double Shear	Triaxial Tension
Stress Analysis	σ_{norm}	P/A_{min}	$0.78\ P/2A_{min}$	P/A_{norm}
	σ_1	σ_{norm}	σ_{norm}	$2.7\sigma_{norm}$
	σ_2	0	0	$0.33\sigma_1$
	σ_3	0	$-\sigma_{norm}$	$0.33\sigma_1$
Stress Parameter	σ_{MPS}	σ_{norm}	σ_{norm}	$2.7\sigma_{norm}$
	σ_e	σ_{norm}	$1.73\sigma_{norm}$	$1.81\sigma_{norm}$
	σ_{PFS}	$2.24\sigma_{norm}$	$2.86\sigma_{norm}$	$4.94\sigma_{norm}$

under multiaxial stress states.

The motivation of the present study is to investigate the high temperature rupture behavior of 5083-Al alloy under different stress states. Attention will be focused on the validity of the aforementioned mechanistic criteria for describing high temperature rupture of this alloy.

2. Experimental Procedures

The material used in this investigation is 5083 aluminum alloy having an average equiaxed grain size of 200 μm. The nominal composition of this alloy is (in wt %) 4.4 Mg, 0.7 Mn, 1.15 Cr, bal. Al. Samples were solid solutionized at 723 K for 6 hr and subsequently air cooled to room temperature. The creep rupture tests were conducted in the air using a constant load machine. The specimens were tested under a maximum tensile stress ranging from 11.7 to 75 MPa at 548±1 K. Three types of high temperature experiments were conducted, each for a different loading configuration. For uniaxial stress state, smooth cylindrical specimens were used (Fig. 1(a)). A tensile load was applied at the ends of the specimen for the uniaxial stress.

For the biaxial stress state, double shear geometry specimens were used. The double shear system is capable of inducing simple shear with moderate strains. The conventional double shear geometry is characterized by the presence of sharp corners at the ends of gage section. Stress concentration at these corners typically results in the development of cracks which gives rise to errors in the overall strain measurement during tertiary creep. In order to avoid this, the gage section with sharp corners was replaced by round notch as shown in Fig. 1(b). We made an assumption that stress concentrations in the gage section are relaxed early in the life of the specimen, and that the steady-state deformation rate should be related to the mean shear stress over the total gage section rather than that at the minimum cross section. The mean shear stress $\bar{\tau}$ for the double shear geometry is given by

$$\bar{\tau}=\frac{P}{\pi\bar{r}^2} \tag{3}$$

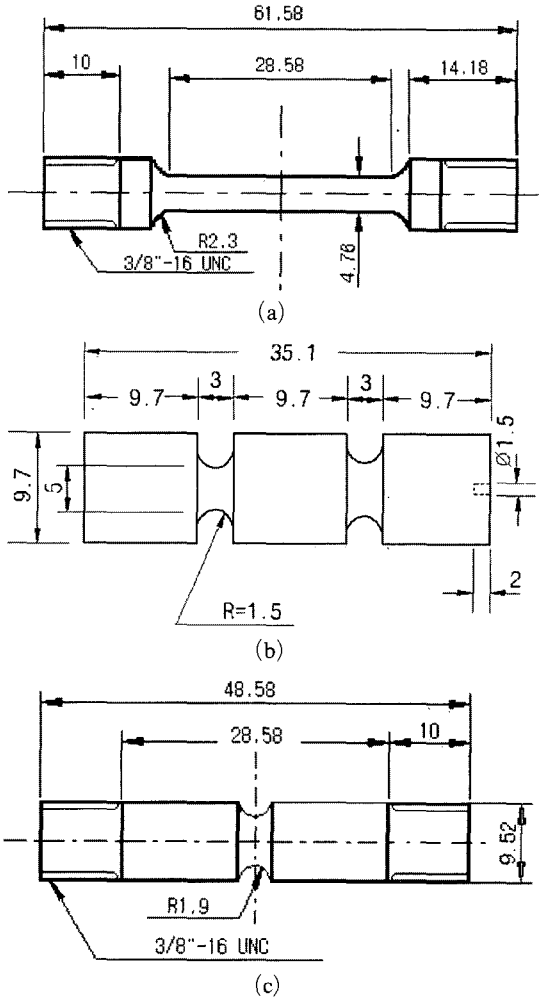

Fig. 1 The specimen geometries and dimensions used the present study: (a) Uniaxial tension, (b) Biaxial double shear and (c) Triaxial tension stresses

where $\bar{r}$ is the mean specimen radius and P is the shear load imposed on each gage section. The mean specimen radius $\bar{r}$ is determined by

$$\bar{r}=\frac{\int_0^R r_s dx}{\int_0^{2R} dx} \tag{4}$$

where r_s is the cross-sectional radius in the shoulders (Fig. 2), and x is the position along the axis of the specimen. The radius in the shoulder is given by

$$r_s=r_{\min}+R-\sqrt{R^2-x^2} \tag{5}$$

Substituting Eq. 5 into Eq. 4 and solving for the integral terms result in

$$\bar{r}=r_{\min}+R-\pi R/4 \tag{6}$$

The value of R and $r_{\min}$ for the current specimen are 1.5 mm and 2.5 mm, respectively. By substituting $0.6r_{\min}$ for R in Eq. 6, we obtain $\bar{r}=1.13r_{\min}$. Finally, the ratio of mean shear stress divided by shear stress at the minimum cross section, $\bar{\tau}/\tau$, is given by

$$\frac{\bar{\tau}}{\tau}=\left(\frac{r_{\min}}{\bar{r}}\right)^2=0.78 \tag{7}$$

The modified round notch double shear specimen has been verified in several works, using experimental and numerical methods (Jonson et al., 1994; Kim et al., 1992).

For triaxial stress conditions, a Bridgman cylindrical specimen with a circular notch in the center was used as shown in Fig. 1(c). Finite element calculations of the steady-state multiaxial stress distributions for this notched bar geometry have been reported by Hayhurst et al.(1977). Their results indicate that once steady-state conditions are reached, the ratio of the maximum principal stress, σ_1, to the remotely applied stress is 2.7 for the remaining life of the specimen. Their results also indicate that the ratio of the maximum principal stress over the effective stress is equal to 1.5 and $\sigma_T=\sigma_2=\sigma_3=0.33\sigma_1$, where σ_T is the transverse stress acting at the notch center.

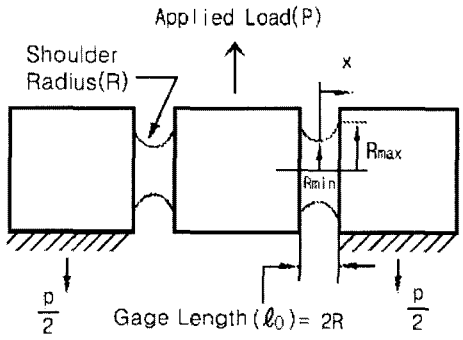

Fig. 2 Geometry of the modified circular notch double specimen

3. Results and Discussion

3.1 Deformation behavior

A series of creep tests conducted at 548 K. Fig. 3, in which true strain is plotted against time, show a typical creep curve obtained for the double shear creep tests at the testing temperature. The true strain and effective stress were converted by using the relationships, $\varepsilon=2/3\gamma$ and $\sigma_e=\sqrt{3}\tau$ (Isshiki et al., 1997). As can be seen in the figure, the creep curve exhibits a deceleration primary creep state (up to 30%) and thereafter the creep behavior is steady state. Then, the curve reaches tertiary stage after 80% of strain. The shape of creep curve is similar to that reported for the aluminum alloys (Kim et al., 1991).

The steady state strain rate against applied stress data for the biaxial shear tests are shown on a double logarithmic plot in Fig. 4. The stress exponent, n, was found to be 5.2, which is in good agreement with the creep results for the 5083-Al alloy reported by others (Inoue et al., 1998). Exact determination of mechanism controlling creep deformation requires further works, but the results imply that, under present testing conditions, 5083-Al alloy exhibits the same characteristics of dislocation climb controlled creep as

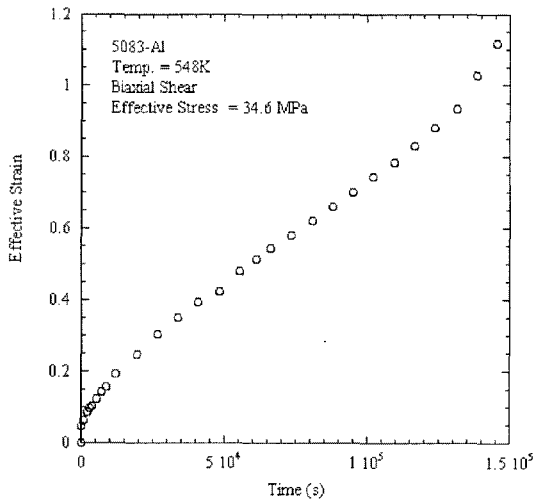

Fig. 3 Typical creep curve for 5083-Al biaxial shear specimen at the effective stress of 34.6 MPa and 548 K

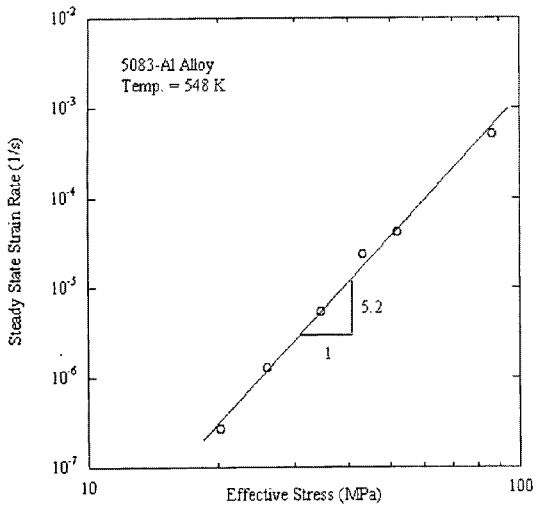

Fig. 4 Steady state strain rate against applied stress for specimen tested under biaxial shear at 548 K

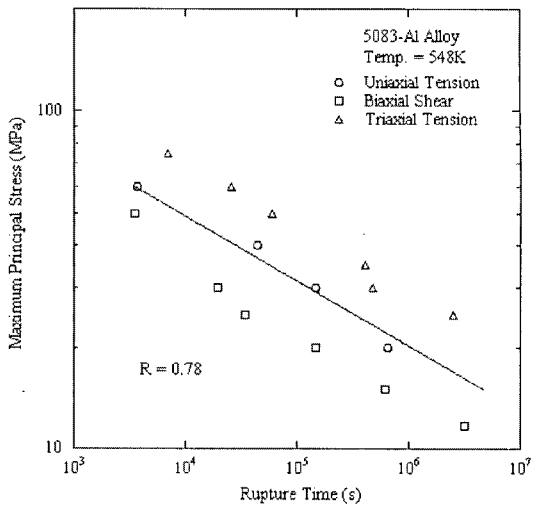

Fig. 5 Maximum principal stress against rupture time for 5083-Al specimens tested at 548 K

observed in pure metals and class II alloys.

3.2 High temperature rupture

The high temperature rupture data for 5083-Al alloy are shown in Fig. 5 as the maximum principal stress plotted against the logarithm of the rupture time. The biaxial data lie below and the triaxial data above the uniaxial tension data. Or, for the same maximum principal stress, a biaxial specimen fails faster than a uniaxial one while a triaxial specimen fails slower than a uniaxial specimen. This implies that a triaxial specimen is stronger than an uniaxial specimen, which means there is a notch strengthening effect.

The notch strengthening effect has been observed in high temperature rupture of other alloys (Nix et al., 1989; El-Nasr et al., 1996). If we consider a cavity applied by the maximum principal stress and other two transverse tensile stresses due to notch geometry, it would be missled that the cavity growth is accelerated with the transverse tensile stresses rather than only the maximum principal stress. However, most of the cavities are located on the grain boundary and the normal stress to the boundary governs cavity growth, driving the cavity absorbing vacancies on the boundary. Also, during grain boundary sliding, the shear stresses on inclined boundaries are relieved, giving rise to a redistribution of normal stresses. Finally, the normal tensile stress on the boundary is amplified, resulting in accelerating cavitaion. Whereas transverse tensile stress acting on the boundary prevents the grain boundary sliding, which results in decreasing the normal stress, causing notch strengthening effect. It seems that if the two transverse stresses are compressively imposed, instead of tensile stresses, they enhance the grain boundary sliding and finally will reduce the rupture time. It can be conceivable that in case of the biaxial shear stress tests, the compressive transverse stress perpendicular to the maximum tensile stress enhances the grain boundary sliding. This causes the rupture time of a biaxial shear specimen shorter than that of an uniaxial tension specimen at the same maximum principal stress. This concept will be more secured through the application of principal facet stress, as shown in Fig. 6. For example, in case of triaxial stress state, if the transverse stress is positive, the final principal facet stress will be reduced, according to Eq. 2. It causes reduction of cavity growth rate. Also, in case of the biaxial shear stress state, one stress component is tensile and the other stress is compressive with the same magnitude. The negative stress component in the second term of Eq. 2 increases the facet stress, enhancing the cavity growth rate.

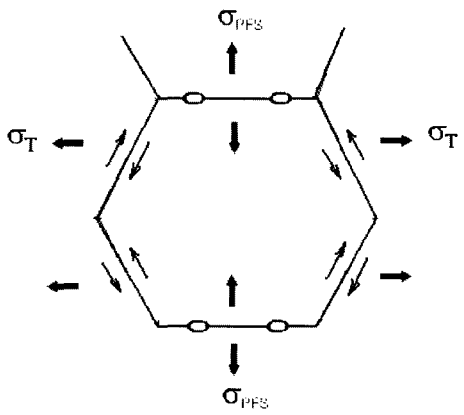

Fig. 6 Reduction of principal facet stress due to suppressing grain boundary sliding by positive transverse tensile stress

The von Mises effective stress is plotted against rupture time for 5083-Al alloy in Fig. 7. This figure shows that the effective stress ($R \approx 0.94$) is successful in bringing the rupture times for different stress states into coincidence. Thus, it seems from these results that creep deformation processes may be dominant in determining the life of the specimens. This result is consistent with the fractographic observations of the relatively deep dimples representating ductile rupture processes as opposed to diffusive cavitation.

The principal facet stress was determined for the data shown in Figs. 5 and 7 and is plotted against rupture time in Fig. 8. It is evident that the principal facet stress ($R \approx 0.96$) correlates the rupture time for the 5083-Al alloy, similar to the von Mises effective stress, bringing the data onto a single curve for the entire range of stresses. The success of the principal facet stress indicates that, under the present experimental conditions, high-temperature fracture is governed by cavitation that is coupled with localized deformation process along inclined directions. In other words, either the grain boundary sliding or the softening processes along the inclined boundaries, rather than the bulk softening processes, could be a significant component of the rupture process. It is reasonable to assume that this localized deformation results in the stress redistribution required for the validity of the principal facet stress.

In attempting to identify mechanisms controlling creep rupture, it is helpful to consider the damage tolerance parameter λ, defined as

$$\lambda = \varepsilon_f / \dot{\varepsilon}_{min} \cdot t_r \tag{8}$$

where ε_f is the rupture strain, $\dot{\varepsilon}_{min}$ is the minimum strain rate, and tr is the time to rupture. Dyson and Leckie (1988) have noted that alloys, which fail by diffusive cavitation and exhibit very little strain softening, generally have λ values that lie between 1 and 2.5. They also suggest that microstructural softening can be a dominant damage

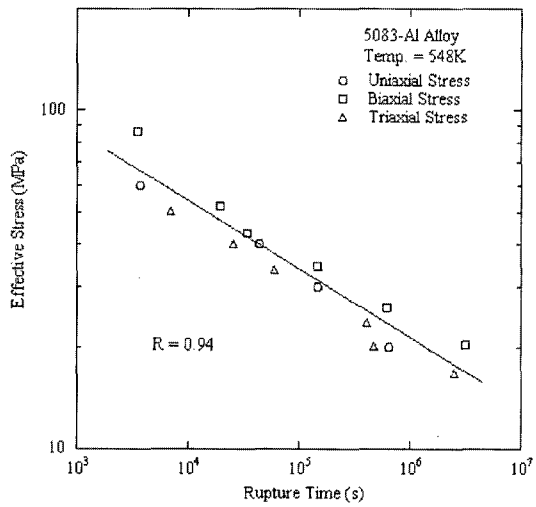

Fig. 7 Effective stress against rupture time for 5083-Al specimens tested at 548 K

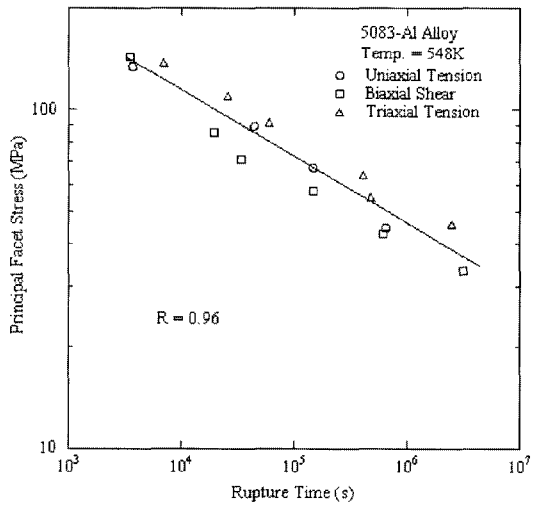

Fig. 8 Principal facet stress against rupture time for 5083-Al specimens tested at 548 K

mechanism when λ takes on larger values (commonly greater than 5). At intermediate levels, the likelihood of an interaction between the two mechanisms exists.

Strain against the product of the minimum strain rate and time, $\dot{\varepsilon}_{min} \cdot t_r$, is plotted in Fig. 9 for 5083-Al specimen tested at 20 MPa under uniaxial tension. Reference lines with slopes representing two values of λ also are shown on this plot. We note that the rupture data in this figure correspond to λ values that are close to 2.72, suggesting that significant microstructural softening has not occurred according to Dyson and Leckie (1988). It should also be noted that the values of λ varies with applied stress. This trend is better illustrated in a plot of λ against maximum principal stress in Fig. 10. The dashed line region represents for the cavitation-controlled region. The data in this figure indicate that λ values range from 1.9 to a maximum of approximately 2.8. Except the value at 40 MPa, the values of λ lie above the cavitation-controlled region but are less than 5, which represents the typical limit which strain softening dominates. It suggests that the creep fracture of the present specimens was generally failed by cavitation rather than bulk microsoftening under the testing conditions and that the cavitation damage causing rupture is more localized.

The success of two parameters, von Mises and principal facet stress, implies that during creep rupture, different mechanisms occur in a coupled manner, with each being dominant for a certain fraction of the creep life. In other words, creep rupture of this alloy under the testing condition is controlled by cavitation coupled with highly localized deformation process, such as grain boundary sliding. It is also conceivable that strain softening controlled the highly localized deformation modes which resulted in cavitation damage in controlling rupture time of this alloy. In

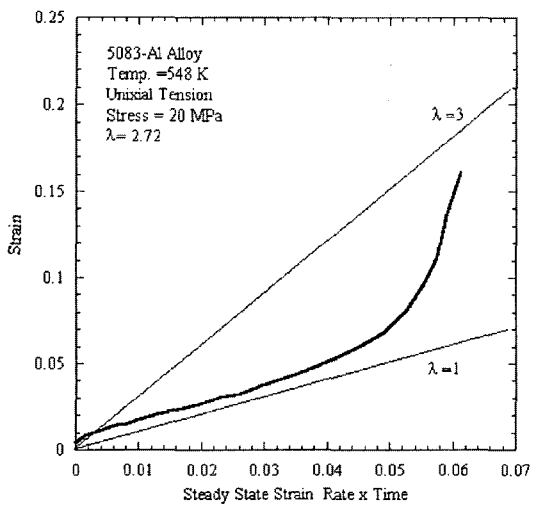

Fig. 9 Strain against time multiplied by the steady state strain rate for 5083-Al specimen at 20 MPa

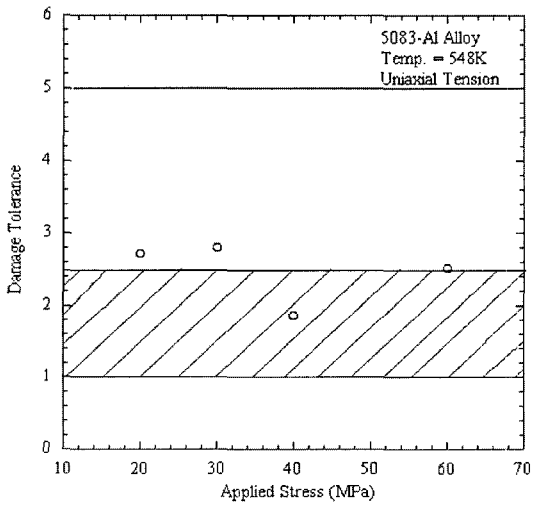

Fig. 10 Damage tolerance (λ) against stress for specimens tested in the present investigation under uniaxial tension

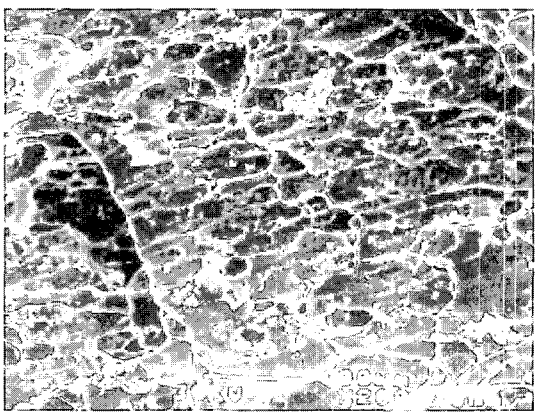

Fig. 11 An SEM micrographs of the rupture surface of a double shear specimen at σ_1=30 MPa

this case, the von Mises effective stress approach is well suited for determining the driving force for strain softening under the multiaxial stress states. Conclusively, it suggests that strain softening in this material is generally an inhomogeneous process that gives rise to stress redistribution in the same way as grain boundary sliding. An SEM micrograph of the rupture surface of a double-shear specimen tested at $\sigma_1=30$ MPa is shown in Fig. 11. This figure shows that this alloy fails in a ductile manner, as characterized by the dimpled nature of the rupture surfaces.

The success or failure of these stresses to correlate the rupture time under multiaxial stresses has been used as a means to identify the governing creep fracture mechanisms. As mentioned previously, the principal stress correlates well with rupture time when failure occurs primarily by unconstrained cavity growth where cavity growth rate is governed only by tensile stress. The effective stress correlates well when the microstructural strain softening occurs during creep or when failure occurs primarily by constrained cavity growth where cavity growth rate is governed only by shear stress. The principal facet stress correlates well when grain boundary sliding causing stress redistribution occurs and when failure occurs primarily by cavitation on transverse boundaries. The current investigation results could be used for the design of high temperature components in nuclear power and chemical plants. Also, it would be expected to be utilized for prediction and evaluation of remaining lifetime and integrity of the components.

4. Conclusions

High temperature rupture data for 5083-Al alloy specimens under multiaxial stress states at 548K have been compared with respect to the maximum principal stress, von Mises effective stress, and the principal facet stress. A high principal facet stress in the double shear specimen and a low principal facet stress in the triaxial notch specimens for the same maximum principal stress imply that different degree of stress redistribution takes place in these specimens. The results indicate that the von Mises effective and principal facet stress give good correlation for the material investigated. The success of two parameters, implies that during creep rupture, different mechanisms occur in a coupled manner, with each being dominant for a certain fraction of the creep life. In other words, creep rupture of this alloy under the testing condition is controlled by cavitation coupled with highly localized deformation process, such as grain boundary sliding. It is also conceivable that strain softening controlled the highly localized deformation modes which resulted in cavitation damage in controlling rupture time of this alloy.

References

Anderson, P. M. and Rice, J. R., 1985, "Constrained Creep Cavitation of Grain Boundary Facets," *Acta Metall.*, Vol. 33, pp. 409~422.

Cane, B. J., 1982, "Creep Damage Accumulation and Fracture Under Multiaxial Stresses," in Advances in Fracture Research (Fracture 81), Vol. 3, pp. 1285~1293, Pergamon Press, Oxford, United Kingdom.

Dyson, B. F., 1976, "Constraints on Diffusional Cavity Growth Rates," *Mater Sci.*, Vol. 10, pp. 349~353.

Dyson, B. F. and Leckie, F. A., 1988, "Physically Based Modeling of Remanent Creep Life," *Mater. Sci. & Eng. A*, Vol. 103, pp. 111~114.

Eggler, G., 1989, "The Effect of Long-Term Creep on Parameter Coarsening in Tempered Martensite Ferritic Steels," *Acta Metall.*, Vol. 37, pp. 3225~3234.

El-Nasr, A. A., Mohamed, F. A., Earthman, J. C., 1996, "High Temperature Rupture of an SiC Particulate Reinforced Al Composite Under Multiaxial Stress State," *Mat. Sci. & Eng. A*, Vol. 214, pp. 33~41.

Goel, A., Ginter, T. J. and Mohamed, F. A., 1983, "Effect of Stress Reduction Ratio on the Stress Exponent and Subgrain Size in an Al-Zn Alloy," *Metal. Trans. A*, Vol. 14, pp. 2309~2318.

Hayhurst, D. R., 1972, "Creep Rupture Under Multi-Axial States of Stress," *J. Mech. Phys. Solids*, Vol. 20, pp. 381~390.

Hayhurst, D. R., Leckie, F. A. and Henderson, J. T., 1977, "Design of Notched Bars for Creep-Rupture Testing Under Tri-Axial Stresses," *Int. J. Mech. Sci.*, Vol. 19, pp. 147~159.

Henderson, J., 1979, "An Investigation of Multi-Axial Creep Characteristics of Metals," *Trans. ASME*, Vol. 101, pp. 356~374.

Huddleston, R. L., 1985, "An Improved Multi-axial Creep-Rupture Strength Criterion," *J. Pressure Vessel Technol.*, Vol. 107, pp. 421~429.

Inoue, M. et al., 1998, "Creep and Creep Rupture of Welded Joints of 5083 Aluminum Alloy Plates," *J. Japan Ins. Light Metals*, Vol. 48, No. 10, pp. 479~483.

Isshiki, K. et al., 1997, "A New Miniature Mechanical Testing Procedure: Application to Intermetallics," *Metal. and Mater. Trans. A*, Vol. 28A, pp. 2577~2582.

Jonson, N. L. and Earthman, J. C., 1994, "Numerical Analysis of Primary Creep Deformation in a Novel Double Shear Specimen Geometry," *J. Testing and Evaluation, JTEVA*, Vol. 22, pp. 111~116.

Kim, H. K., Mohamed, F. A. and Earthman, J. C., 1992, "A Novel Specimen Geometry for Double Shear Creep Experiments," *J. Testing and Evaluation, JTEVA*, Vol. 19, pp. 93~96.

Kim, H. K., Chung, K. and Chung, C. S., 1998, "High Temperature Rupture Lifetime of 304 Stainless Steel Under Multiaxial Stress States," *KSME Journal A*, Vol. 22. No. 3, pp. 595~602.

Nix, W. D. et al., 1989, "The Principal Facet Stress as a Parameter for Predicting Creep Rupture Under Multiaxial Stresses," *Acta Metall.*, Vol. 37, pp. 1067~1077.

Ridel. H., 1987, "Fracture at High Temperatures," Berlin, Springer.

Vetrano, J. S., Lavender, C. A., Hamilton, C. H., Smith, M. T. and Bruemmer, S. M., 1994, "Superplastic Behavior in a Commercial 5083 Aluminum Alloy," *Scripta Metall.*, Vol. 30, pp. 565~570.